Solvation Dynamics and Adsorption on Ag Hydrosols of Oxazole: A Raman and Computational Study†

Marco Pagliai,‡ Maurizio Muniz-Miranda,‡,§ Gianni Cardini,‡,§ and Vincenzo Schettino*,‡,§

Dipartimento di Chimica, Università di Firenze, via della Lastruccia 3, 50019 Sesto Fiorentino, Italia, and European Laboratory for Nonlinear Spectroscopy (LENS), via Nello Carrara 1, 50019 Sesto Fiorentino, Italia

Received: June 12, 2009; Revised Manuscript Received: August 21, 2009

The interactions between oxazole and water or silver nanoparticles in aqueous dispersions have been studied with a computational approach based on ab initio molecular dynamics simulations, with the Car−Parrinello method, and density functional calculations in combination with Raman and surface enhanced Raman scattering (SERS) experiments. The solvation dynamics of oxazole in water allowed for the characterization of the hydrogen bond between water and solute, which has been shown to occur essentially through the nitrogen atom of the heterocyclic molecule. To mimic the solvation process or the adsorption on silver and interpreting the corresponding Raman and SERS spectra in aqueous solution or in Ag hydrosols, density functional calculations have been carried out on model systems made up by oxazole bound to water molecules or to positively charged silver clusters. Also, the chemisorption on Ag nanoparticles is found to occur by means of the nitrogen atom of oxazole interacting with the metal substrate.

Introduction

The interaction between metal nanoparticles in aqueous dispersions and different species, in particular, organic molecules containing heteroatoms, is a topic that has received particular attention in recent years,[1−3] for possible technological applications, for example, in heterogeneous catalysis. The adsorption and the mechanism involved in the chemical processes at the metal surface can be conveniently monitored by means of the surface enhanced Raman scattering (SERS).[4−6] Although an exhaustive explanation of the enhancement mechanism has not yet been achieved,[7] the enhancement of the Raman spectra of organic molecules adsorbed on noble metal nanoparticles can be attributed to two contributions: the electromagnetic mechanism, related to the excitation of the electrons localized at the metal surface, and the chemical mechanism, based on a resonance effect involving the energy levels on both metal and molecule. The electron excitation for metal nanoparticles can be observed as surface plasmon resonance (SPR) bands in the UV−visible absorption spectrum. For example, silver nanoparticles (with 10−20 nm average diameters) in aqueous colloidal dispersions show an intense SPR band at ∼400 nm. Under chemisorption of organic molecules on the silver colloidal surface, the aggregation of nanoparticles gives rise to a second SPR band at longer wavelengths. Actually, for chemisorbed molecules, the two SERS mechanisms act simultaneously in a synergic way giving rise to enhancement factors of 10^6 or more with respect to the Raman effect of the nonadsorbed molecules. In single-molecule measurements, the SERS enhancement was evaluated to reach $10^{14}-10^{15}$ factors.[6,8] The chemical contribution, albeit evaluated[9,10] up to 10^2, is however important in the SERS, because it induces marked frequency shifts and relative intensity changes of the observed bands.

The adsorption process on silver nanoparticles in aqueous dispersion cannot be fully understood if the action of the water molecules of the surrounding medium on the ligand molecules is neglected. Hence, the purpose of the present work is to analyze the Raman spectra of an organic molecule, oxazole, either in water solution or chemisorbed on silver colloidal nanoparticles. Density functional theory (DFT)[11,12] calculations on the structural and vibrational properties have been carried out on complexes of oxazole with water molecules or with silver clusters. A preliminary study of the solvation dynamics of oxazole in water has been performed by ab initio Car−Parrinello molecular dynamics simulation (CPMD).[13−16] The O−H···N hydrogen bond has been characterized and DFT calculations of the Raman spectra of oxazole in water have been performed on an oxazole/water complex to interpret the solvation process. The active sites of the silver colloidal particles for the chemisorption of oxazole have been modeled with Ag^+ ions or Ag_3^+ clusters. In agreement with previous works on the pyridine chemisorption,[17,18] the adsorption on silver clusters could be considered able to reproduce the Raman frequency shifts of oxazole from the aqueous solution to the silver colloidal dispersion. The SERS intensities are obtained by a DFT approach adopting this model system, albeit they also depend on the electromagnetic mechanism, as well as that found for pyrazole in Ag hydrosols.[19] This can be justified by considering that the chemical effect is really predominant for the SERS profiles, as stated by Otto.[20] In addition, the actual existence of Ag_3^+ clusters, which act as surface active sites for the chemisorption of ligands, was recently ascertained in silver colloidal dispersions.[21]

Oxazole (see Figure 1) has been chosen as a probe molecule for this investigation as a prototype of a class of heterocyclic compounds with basic importance in natural products, medicinal chemistry and materials science, as evidenced by the continued growth in the number of research publications and reviews.[22] In addition, oxazole is a sufficiently small molecule to allow for quite sophisticated calculations like those based on CPMD and DFT approaches.

† Part of the "Vincenzo Aquilanti Festschrift".

* To whom correspondence should be addressed. E-mail: vincenzo.schettino@unifi.it.

‡ Dipartimento di Chimica, Università di Firenze.

§ European Laboratory for Nonlinear Spectroscopy.

10.1021/jp905530x
Published on Web 09/21/2009

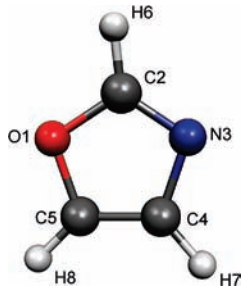

Figure 1. Molecular structure of oxazole.

Computational Details

The solvation dynamics of oxazole in water has been studied by Car−Parrinello molecular dynamics simulations, whereas the structural and spectroscopic properties have been obtained by DFT calculations on single molecules or model complexes with the Gaussian suite of programs.[23] A detailed description of the calculations performed in the present study are reported in the following.

Car−Parrinello Molecular Dynamics Simulations. The solvation dynamics of oxazole in water has been studied by Car−Parrinello molecular dynamics simulations[13−16] using the CPMD[24] code in conjunction with the BLYP[25,26] exchange and correlation functional, using norm conserving Martins-Troullier pseudopotentials[27] along with the Kleinman-Bylander[28] decomposition and a plane wave expansion truncated at 70 Ry. Deuterium atoms have been used instead of hydrogen to allow for a larger time step.

The sample, made up of 1 oxazole molecule and 64 water molecules in a periodic cubic box with sides 12.6578 Å (at the experimental density of deuterated water, 1.1056 g·cm^{-3}), has been thermalized at 300 K for ∼3.5 ps by velocity scaling. The trajectory has been collected for ∼15.7 ps (saving the coordinates at every step) with a time step of 5 au (0.12 fs) in the NVE ensemble. The fictitious electronic mass was 700 au to allow for an acceptable decoupling between electronic and nuclear degrees of freedom.

Density Functional Theory Calculations. The DFT calculations[11,12] have been performed with the Gaussian suite of programs,[23] using a combination of the BLYP[25,26] and B3LYP[29−31] exchange and correlation functionals along with the LANL2DZ,[32−34] 6-31G(d), 6-31++G(d,p), and 6-311++G(d,p) basis sets.[35,36] In the calculations on the silver/oxazole complexes, the LANL2DZ basis set has always been adopted for the Ag atomic species. Structure optimizations of the oxazole molecule, of the water/oxazole complex, and of the silver/oxazole systems have been carried out with a very tight criterion, and normal frequency calculations have been performed using an improved grid in the numerical evaluation of the integrals, INTEGRAL(GRID = 199974). The calculated frequencies have been uniformly scaled. The scaling factors adopted have been optimized to reproduce the experimental findings with the best agreement and have values very close with those adopted in previously studied aromatic systems.[17−19]

The Raman intensities of the vibrational modes, computed on the basis of the double harmonic approximation, that is, without taking into account the electric and mechanical anharmonicity, correspond to spatially averaged values according to the usual formulas reported in standard textbooks.[37]

Experimental Section

Following the procedure proposed by Creighton et al.[38] the Ag hydrosols have been prepared by adding $AgNO_3$ (99.9999% purity, Aldrich) to excess $NaBH_4$ (99.9% purity, Aldrich). The ligand adsorption was obtained by adding oxazole (98.0% purity, Aldrich) to silver colloids in 10^{-3} M concentration. NaCl (99.999% purity, Aldrich) was added to Ag colloids in 10^{-3} M concentration to improve the SERS enhancement. Since this procedure leads to SERS spectra showing a weak ligand−metal interaction,[39] another sample has been prepared by perfoming the same reduction of silver ions but in the presence of 10^{-3} M oxazole. In such a way, we obtained a colloidal dispersion with oxazole-capped Ag nanoparticles. No reduction of oxazole has been observed.

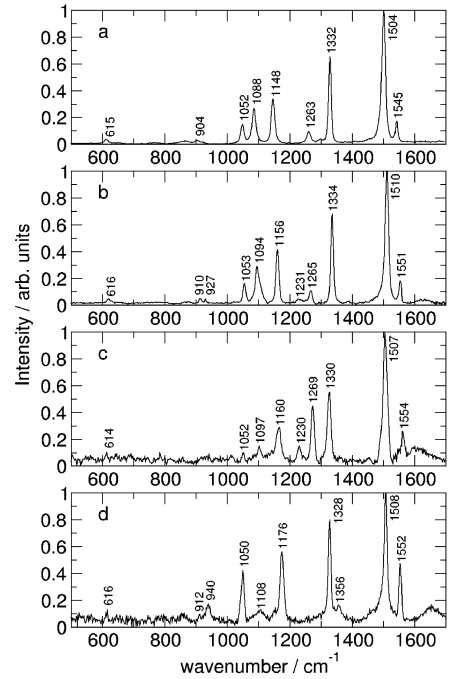

Figure 2. Raman spectra of oxazole: (a) in pure liquid, (b) in aqueous solution, (c) physisorbed on Ag hydrosol, and (d) chemisorbed on Ag hydrosol.

Raman spectra were recorded using the 514.5 nm line of a Coherent argon ion laser, a Jobin-Yvon HG2S monochromator equipped with a cooled RCA-C31034A photomultiplier, and a data acquisition facility. To impair the thermal effects due to the laser light, a defocused beam with low power (20 mW) was used. Power density measurements were performed with a power meter instrument (model 362; Scientech, Boulder, CO) giving ∼5% accuracy in the 300−1000 nm spectral range.

Raman and SERS Spectra. Figure 2 shows the Raman spectra of oxazole as pure liquid (a), in water solution (b), and in the presence of silver nanoparticles (c,d). It has been observed[39] that oxazole, added to silver sols prepared according to the Creighton's procedure,[38] interacts only weakly or physisorbs, as shown by the spectrum reported in panel c of Figure 2, where small frequency-shifts occur with respect to the corresponding normal Raman bands in the liquid or in water solution. However, performing the reduction of the silver ions in the presence of oxazole, Ag nanoparticles capped with oxazole molecules have been obtained. In these conditions, a SERS spectrum has been obtained (panel d of Figure 2) with different relative intensities and larger frequency shifts.

The Raman spectra in the range between 500 and 1700 cm^{-1} are dominated by an intense band at ∼1505 cm^{-1}, attributed to a combination of C═N and C═C stretching modes. The chemical interaction of oxazole with Ag nanoparticles determines significant frequency shifts with respect to the pure liquid.

Marked shifts, confidently due to the chemisorption of oxazole, are observed for the bands at 940, 1108, and 1176 cm^{-1} in the SERS spectrum, as shown in Figure 2d.

Results and Discussion

The Raman spectra of oxazole in aqueous solution or adsorbed on silver colloidal particles can be obtained by DFT calculations, adopting a model system made up of the heterocyclic molecule bound to (one or more) solvent molecules or to small positively charged Ag clusters. In fact, by adopting a similar computational approach, the Raman frequencies and intensities of pyridine were correctly reproduced, both in solution and in Ag hydrosol.[17] The number of water molecules H bonded to pyridine was obtained through a classical molecular dynamics simulation. The study of the solvation dynamics of oxazole in water with classical molecular dynamics is more complicated, because of the presence in the ring of two heteroatoms (nitrogen and oxygen atoms) with lone pairs, making the development of a force field based on a point charge model for the electrostatic part a difficult task, as stated by McDonald et al.[40] For these reasons, the approach adopted in the present study is based on ab initio molecular dynamics simulations, using the Car−Parrinello method,[13−16] which overcomes this difficulty, calculating the forces by a DFT approach during the simulation. The CPMD simulations have been performed adopting the BLYP[25,26] exchange and correlation functional, which has shown to be particularly suitable in the study of H bonded systems, like pure liquids (for example, water[41,44] and methanol[45,46]) and ions or molecules in solutions.[16,47]

In order to develop a simplified model that considers only the main features of the real system, it is necessary to analyze the solute−solvent interactions. The first insight on the structural reorganization of the water molecules around oxazole has been obtained from the pair radial distribution functions, $g(r)$, reported in Figure 3a, for the N···H and O···H contacts.

It is interesting to observe that the oxygen atom of oxazole gives rise only to extremely weak interactions with the aqueous medium, whereas the nitrogen atom is involved in the formation of one H bond. This behavior can be rationalized by considering that in ab initio calculations, both with HF and DFT approaches, the electrostatic potential (ESP) partial charges on the nitrogen atom result significantly more negative than those on the oxygen atom. In particular, the ESP charges on the nitrogen atom are −0.59 and −0.51 e at HF/6-31G(d) and B3LYP/6-31G(d) level of theory, respectively, whereas those on the oxygen atom are −0.26 and −0.20 e. Similar results were obtained by McDonald et al.[40] The present CPMD results are particularly helpful, allowing to simplify the model for the successive DFT calculations, taking into account only one water molecule bound to the nitrogen atom.

In order to state the directional character of the H bond[48] between oxazole and water, the angular distribution function has been reported in Figure 3b, showing that the distribution extends up to ∼30°, a value similar to that found in water and methanol.[45,49]

Figure 4 shows the spatial distribution function (SDF)[50] related to the N···H contact. The isosurface close to the nitrogen atom of oxazole represents 90% probability to find a water molecule bound to the nitrogen atom of the heterocycle. The region spanned by the water molecules bound to oxazole is relatively small, suggesting a stable H bond.

In order to obtain additional information on the configurational space and dynamics of the H bond, the simulation trajectory has been analyzed in terms of a recently introduced

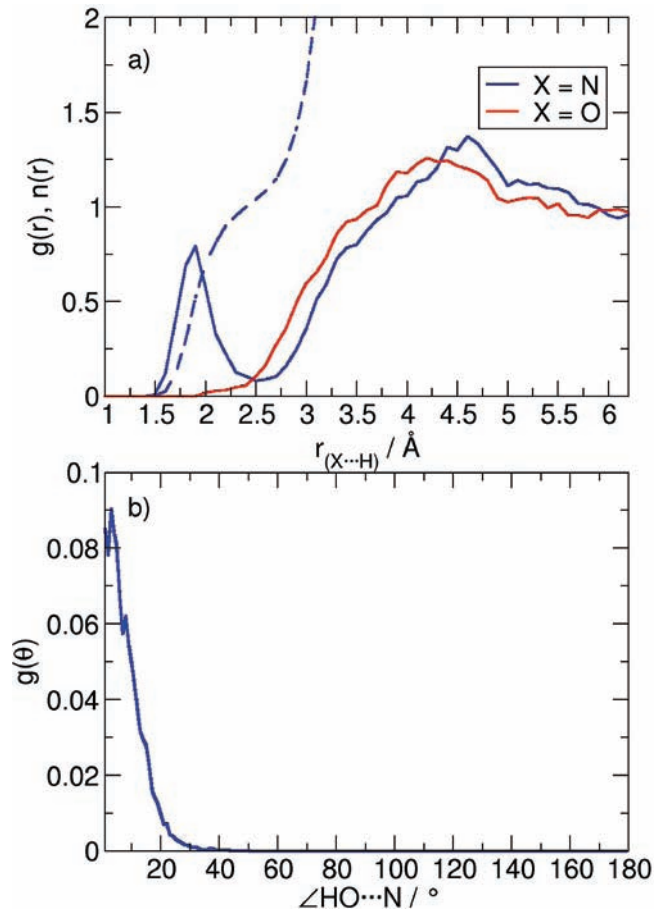

Figure 3. (a) Radial distribution function (full blue line) and running integration number (dashed blue line) for the N···H contact; the red line reports the radial distribution function of O···H contact, showing only a weak interaction with the solvent. (b) Angular distribution function for the H−O···N angle.

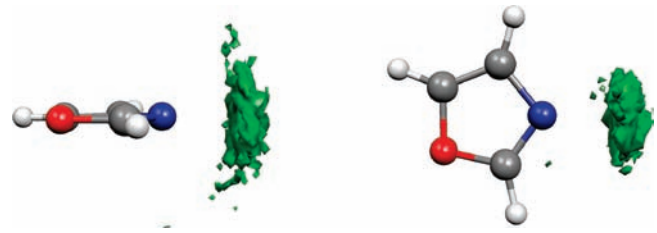

Figure 4. Spatial distribution along two different views of the H bonded water molecules around the nitrogen atom of oxazole.

function F_j^{HB}, which has been adopted with success in the study of the H bond of methanol,[45] chloride and bromide ions in methanol,[51,52] and pyridine in water.[17]

The function is defined as

$$F_j^{HB} = A(r(t)) \cdot B(\theta(t)) \tag{1}$$

with $A(r(t))$ and $B(\theta(t))$ given by

$$\begin{cases} A(r(t)) = e^{-(r_e - r_j(t))^2/(2\sigma_r^2)} & \text{if } (r_e - r_j(t)) < 0 \\ A(r(t)) = 1 & \text{if } (r_e - r_j(t)) \geq 0 \\ B(\theta(t)) = e^{-(\theta_e - \theta_j(t))^2/(2\sigma_\theta^2)} & \text{if } (\theta_e - \theta_j(t)) < 0 \\ B(\theta(t)) = 1 & \text{if } (\theta_e - \theta_j(t)) \geq 0 \end{cases}$$

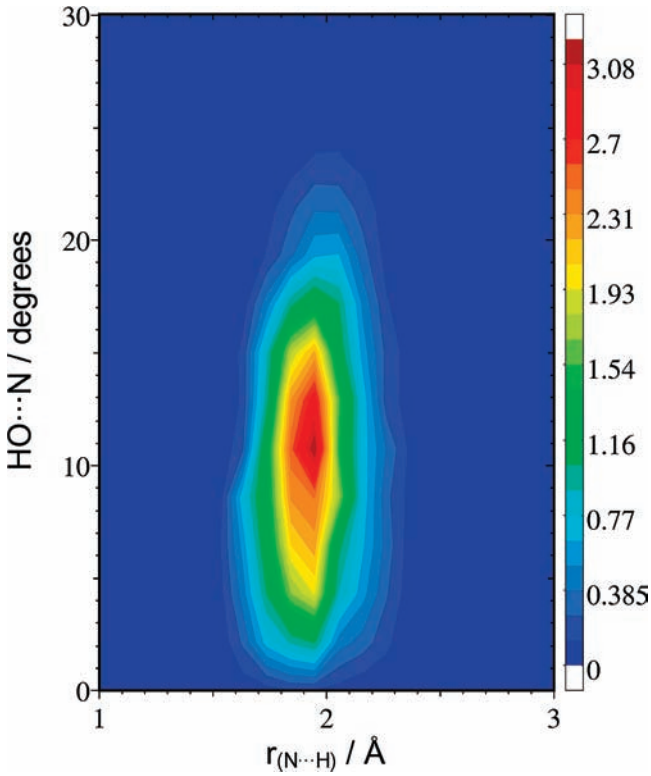

Figure 5. H bond configurational space obtained as weighted $g(r,\theta)$ function from eq 1.

The values of the parameters r_e, θ_e, σ_r, and σ_θ are directly extracted from the unnormalized pair radial, $h(r)$, and angular, $h(\theta)$, distribution functions. In the above definitions, r_e is the position of the first peak in $h(r)$, and θ_e is the position of the first peak in $h(\theta)$, whereas σ_r and σ_θ are the half widths at half-maximum in $h(r)$ and $h(\theta)$, respectively. $r_j(t)$ and $\theta_j(t)$ are the instantaneous distance and angle values involved in the interaction between the water molecule j and the nitrogen atom of oxazole.

The F_j^{HB} function assumes values close to 1 for strong H bond interactions, whereas it goes rapidly to 0 as $r_j(t)$ and $\theta_j(t)$ are greater than the reference values r_e and θ_e, respectively. Values of F_j^{HB} lower than 10^{-4} have been considered arbitrarily as zeros.

The directional character of the H bond interaction can be appreciated in Figure 5, where the structural information related to the F_j^{HB} function is collected in the form of a weighted $g(r,\theta)$ function. Figure 6 shows the dynamical features of the H bond.

The upper panel of Figure 6 monitors the water molecules H bonded to oxazole during the CPMD simulation. At each time step, a point on the graph is reported if the corresponding water molecule forms a H bond with oxazole. It can be seen that along most of the simulation run the water molecule with index #12 is involved in the H bond, with only a small number of contacts related to other water molecules that weakly interact with the nitrogen atom of oxazole. Nevertheless, observing the central panel of Figure 6, where the time-dependence of F_{12}^{HB} has been reported, it is possible to note that the H bond forms and breaks continuously, although for short time intervals. This description is particularly interesting, since eq 1 allows one to correctly take into account the vibrations of the water molecule in the process of formation and breaking of the H bond. In the bottom panel of Figure 6, it is possible to observe that only one hydrogen atom of the water molecule with index #12 is actually involved in the H bond with oxazole. This constitutes an explanation for the small amplitude of the motion observed in

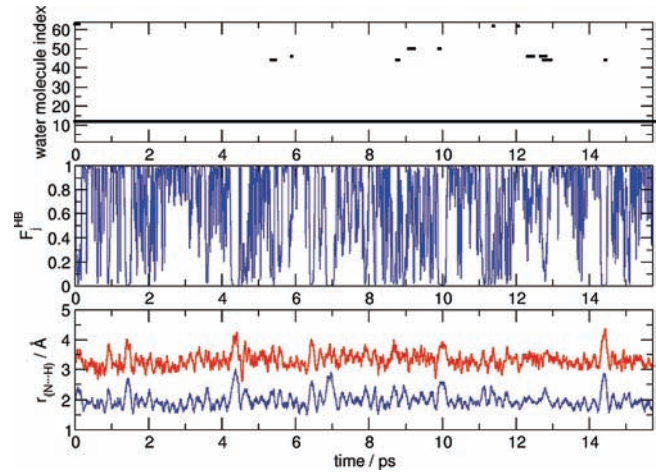

Figure 6. Upper panel: Water molecules H bonded to the solute during the CPMD simulation. All of the solvent molecules in the sample are labeled from 1 to 64. The graph identifies the molecules directly H bonded to oxazole at each time step. Central panel: Evolution of F_j^{HB} for the molecule #12. Lower panel: N···H distance as a function of time for the hydrogen atoms of water molecule #12.

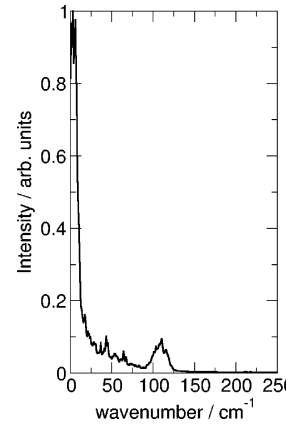

Figure 7. Fourier transform of the N···H-stretching mode obtained by CPMD simulations.

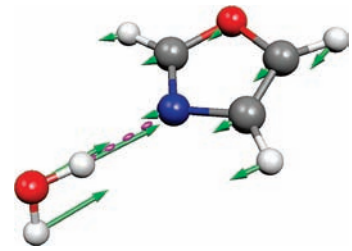

Figure 8. Intermolecular N···H stretching mode obtained by DFT calculations at B3LYP/6-311++G(d,p) level of theory on the fully deuterated system for a direct comparison with CPMD simulations.

the spatial distribution function, reported in Figure 4. In considering that only one water molecule is hydrogen bonded to the nitrogen atom of oxazole, the Fourier transform of the N···H bond length function gives the frequency of the water/oxazole intermolecular vibration. The result is reported in Figure 7 showing that the N···H stretching frequency occurs at ~120 cm^{-1}. A representation of the corresponding normal mode, as reported in Figure 8, has been obtained from the calculation at the B3LYP/6-311++G(d,p) level of theory for the fully deuterated water/oxazole dimer. By adopting this model, the N···H stretching frequency occurs at 139 cm^{-1}, a value very close to that obtained for pyridine and diazines[53] using a similar

TABLE 1: Salient Structural Parameters of Oxazole Molecule[a]

		A		*B*		*C*		*D*	
	exptl[57]	BLYP	B3LYP	BLYP	B3LYP	BLYP	B3LYP	BLYP	B3LYP
r_{12}	1.357	1.425	1.400	1.378	1.358	1.380	1.359	1.378	1.357
r_{23}	1.291	1.326	1.313	1.307	1.294	1.308	1.295	1.303	1.290
r_{34}	1.396	1.430	1.417	1.404	1.392	1.405	1.393	1.403	1.392
r_{45}	1.353	1.384	1.372	1.367	1.356	1.369	1.357	1.364	1.353
r_{51}	1.369	1.424	1.406	1.388	1.371	1.390	1.373	1.387	1.370
r_{26}	1.075	1.085	1.077	1.087	1.080	1.086	1.080	1.084	1.078
r_{47}	1.075	1.086	1.078	1.088	1.081	1.087	1.080	1.084	1.078
r_{58}	1.073	1.084	1.076	1.085	1.078	1.084	1.078	1.082	1.076
θ_{123}	115.0	113.5	113.2	115.0	114.8	114.6	114.5	114.5	114.5
θ_{234}	103.9	105.2	105.4	103.9	104.0	104.2	104.3	104.4	104.3
θ_{345}	109.0	109.6	109.3	109.5	109.3	109.4	109.2	109.3	109.1
θ_{451}	108.2	107.9	107.6	108.0	107.8	107.9	107.7	107.9	107.8
θ_{512}	103.9	103.8	104.5	103.7	104.1	103.9	104.3	103.9	104.3

[a] For the numbering of atoms see Figure 1. Distances in Å and angle in degrees. *A* = B3LYP/LANL2DZ, *B* = B3LYP/6-31G(d), *C* = B3LYP/6-31++G(d,p), *D* = B3LYP/6-311++G(d,p).

TABLE 2: Calculated Frequencies with BLYP and B3LYP Functionals and *G* = 6-311++G(d,p) Basis Set, Compared with Experiments in the Liquid Sample (This Work) and in the Gas Phase[58] [a]

$\nu_{exp.}$liquid	$\nu_{exp.}$[58]	symm.	assignment[b]	BLYP/G	B3LYP/G
615	604	A″	ring tors	617	612
	646	A″	ring tors	659	650
	749	A″	CH wag	741	749
	832	A″	CH wag	804	822
	859	A″	ring def	853	861
	899	A′	ring def	909	902
904	909	A′	CH wag	915	914
1052	1052	A′	C−O str + CH bend	1046	1051
1088	1081	A′	C−O str + C−N str	1051	1073
	1091	A′	C−N str + O−C str	1103	1100
1148	1143	A′	O−C str + CH bend	1147	1141
1263	1260	A′	CH bend	1269	1251
1332	1330	A′	CH bend	1338	1333
1504	1509	A′	C═N str + C═C str + CH bend	1502	1499
1545	1545	A′	C═C str + C═N str	1549	1548

[a] Scaling factors of 1.031 and 0.984 have been used for BLYP and B3LYP, respectively. [b] tors = torsion, wag = wagging, def = deformation, str = stretching, bend = bending.

TABLE 3: Calculated and Observed Frequencies for Oxazole in Water and in Ag Colloid[a]

water	H_2O/oxazole		colloid	Ag^+/oxazole		Ag_3^+/oxazole	
$\nu_{exp.}$	BLYP/G	B3LYP/G	$\nu_{exp.}$	cBLYP/G	B3LYP/G	BLYP/G	B3LYP/G
616	618	612	616	618	613	619	613
910	916	908	912	911	905	915	908
927	928	923	940	962	954	959	950
1053	1045	1049	1050	1041	1049	1043	1050
1094	1073, 1107	1087, 1103	1108	1105, 1137	1098, 1124	1104, 1127	1098, 1118
1156	1152	1149	1176	1191	1202	1177	1186
1265	1269	1252		1279	1262	1277	1259
1334	1339	1334	1328	1332	1327	1334	1330
			1356				
1510	1504	1500	1508	1501	1502	1502	1502
1551	1556	1553	1552	1567	1559	1565	1558

[a] The adopted basis set is *G* = 6-311++G(d,p).

computational approach and very close to that observed in both experiments and simulations in liquid water.[54−56]

On the basis of the computational results regarding the solvation of oxazole, the Raman and SERS spectra of oxazole in water solution and chemisorbed on silver colloidal particles have been computed with DFT calculations using the BLYP and B3LYP exchange and correlation functionals. The choice of these functionals is justified by the following considerations. The BLYP functional has been used in the CPMD simulation, whereas the B3LYP functional is able to satisfactorily reproduce the structural parameters of oxazole, as shown in Table 1. In addition, B3LYP has previously been found as one of the most effective functionals to reproduce the Raman or SERS spectra of heterocyclic systems.[17,18]

In particular, bond lengths and angles are better reproduced by adopting the more extended 6-311++G(d,p) basis set, which has been hereafter adopted for the Raman vibrational calculations. All DFT calculations have been performed on the isolated molecule, on the H_2O/oxazole complex, and on Ag^+/oxazole and Ag_3^+/oxazole systems.

The experimental and calculated Raman frequencies of oxazole are reported in Table 2. DFT calculations with the

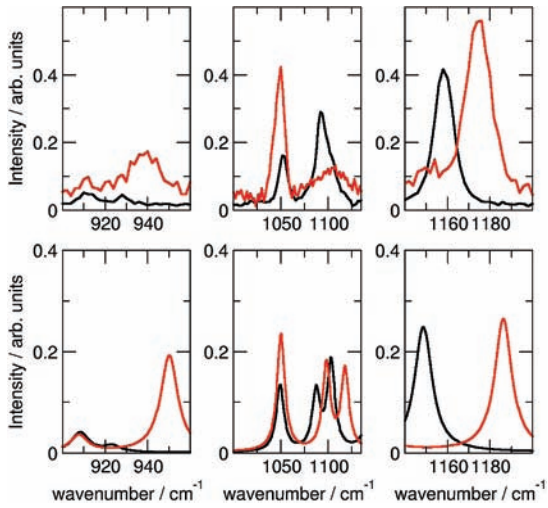

Figure 9. Details of the experimental (upper panel) and calculated (lower panel) Raman (black line) and SERS (red line) spectra close to 900, 1000, and 1100 cm^{-1} of oxazole in water and adsorbed on Ag hydrosols.

B3LYP functional provide a more satisfactory agreement than those with BLYP, as expected. It can be noted, for clarity of the following discussion, that the 1073−1100 cm^{-1} doublet is not resolved in the Raman spectrum of the liquid sample.

DFT/B3LYP calculated frequencies for H_2O/oxazole and Ag_3^+/oxazole model systems are reported in Table 3 and compared with the experimental values. It is remarkable that the most significant shifts of the Raman peaks at 904, 1088, and 1148 cm^{-1} on going from water to silver colloid are accurately reproduced in the calculations (see Figure 9). Also, the relative intensities appear satisfactorily reproduced in the calculations.

A more complete comparison of the experimental and calculated Raman and SERS spectra is reported in Figure 10 and in Figure 11 using the BLYP and B3LYP functionals, respectively. A better overall performance of the latter functional can be noted. By adopting the Ag_3^+ cluster instead of the Ag^+ ion, a significant improvement of the agreement between simulated and experimental SERS spectra is obtained for both band frequencies and intensities.

According to the Ag_3^+/oxazole model, the ligand adsorbs on silver through the nitrogen atom, with the plane of the molecule perpendicular to the surface of the colloidal particle. The structure of the Ag_3^+/oxazole complex is shown in Figure 12. In this respect, the Ag_3^+ cluster can represent an atomic-size defect of the colloidal surface, where the apical atom interacts with the molecule and the other two atoms are encapsulated in the bulk lattice.

Conclusions

In the present work, we have attempted an interpretation of the frequency shifts and of the relative intensities observed in the SERS of oxazole adsorbed on silver colloidal dispersion. To this purpose, the SERS spectra have been compared with the Raman spectra of oxazole in water solution. Ab initio molecular dynamics simulations in the Car−Parrinello approach have been carried out for the solvation process of oxazole in water, showing that a stable hydrogen bonded H_2O/oxazole complex is formed where oxazole is bound through the nitrogen atom. DFT calculations have been carried out on the H_2O/oxazole complex providing a Raman spectrum in agreement with that observed in aqueous solution. The SERS spectrum of

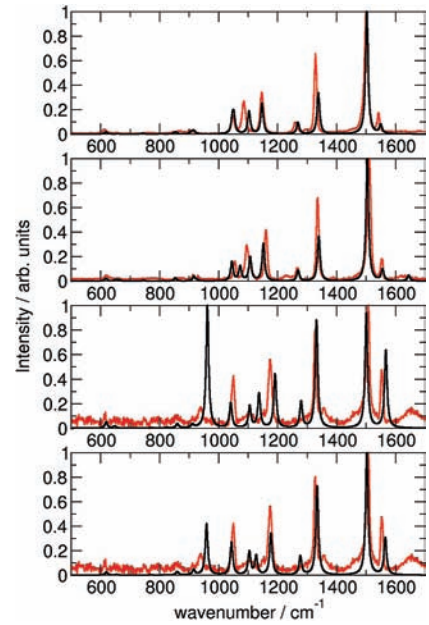

Figure 10. Calculated Raman spectra of (from top to bottom) oxazole, H_2O/oxazole, Ag^+/oxazole, and Ag_3^+/oxazole. The DFT calculations have been performed using the 6-311++G(d,p) basis set of C, N, O, and H atoms and LANL2DZ for Ag atoms with the BLYP functional. The experimental Raman spectra (from top to bottom) of liquid oxazole, oxazole in water, and oxazole chemisorbed on silver are reported for comparison (red line).

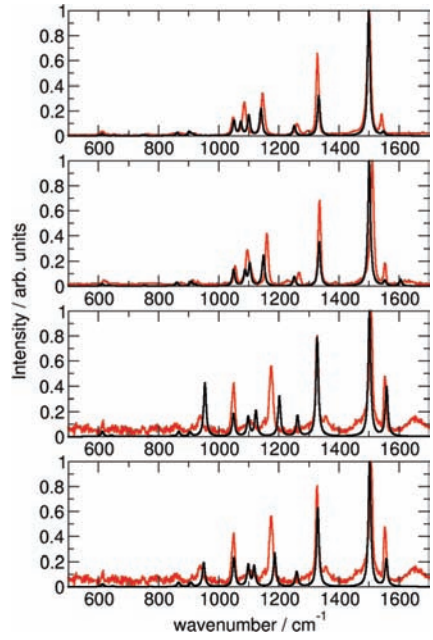

Figure 11. Calculated Raman spectra of (from top to bottom) oxazole, H_2O/oxazole, Ag^+/oxazole, and Ag_3^+/oxazole. The DFT calculations have been performed using the 6-311++G(d,p) basis set of C, N, O, and H atoms and LanL2DZ for Ag atoms with the B3LYP functional. The experimental Raman spectra (from top to bottom) of liquid oxazole, oxazole in water, and oxazole chemisorbed on silver are reported for comparison (red line).

oxazole chemisorbed on silver nanoparticles has been modeled assuming that the oxazole molecule interacts with Ag_3^+ cluster through the nitrogen atom with a configuration perpendicular to the nanoparticle surface. This model reproduces accurately the observed SERS spectrum, particularly concerning the most significant frequency shifts and the relative intensity changes.

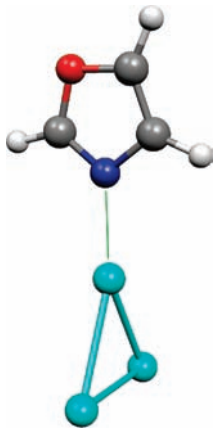

Figure 12. Optimized structure of oxazole bonded to the Ag_3^+ cluster.

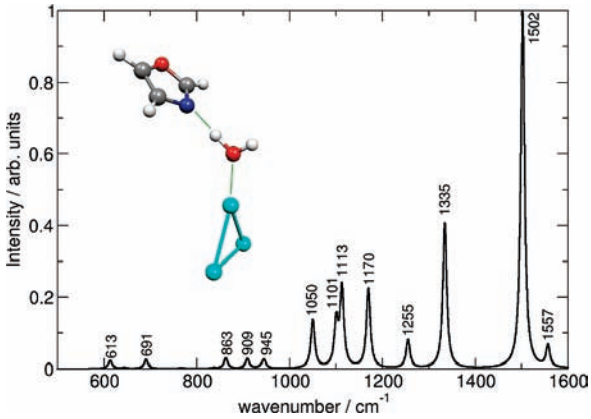

Figure 13. Calculated SERS spectrum of the silver/water/oxazole complex with the corresponding optimized structure.

In conclusion, the chemisorption process of oxazole onto the silver colloidal substrate occurs by replacing the water molecule bound to the nitrogen atom of the heterocycle with a positively charged active site of the metal surface. Actually, the calculated binding energy (BSSE corrected)[35,59] for the Ag_3^+/oxazole complex is much larger (-123.07 kJ·mol^{-1}) than that calculated for the H_2O/oxazole complex (-23.92 kJ·mol^{-1}). When, instead, oxazole physisorbs on silver, the interaction with the colloidal substrate is mediated through the water molecule, which remains bound to oxazole. This fact explains the small frequency shifts in the SERS spectrum of physisorbed oxazole compared with those in the Raman spectrum of oxazole in aqueous solution.

An attempt has been made to describe the physisorption process, performing DFT calculations on the model reported in Figure 13. The optimization procedure has allowed us to identify a new stable structure where the interaction of oxazole with the nanoparticle is mediated by the water molecule (the equilibrium N···Ag distance is 4.43 Å). The calculated Raman spectrum of oxazole/water/Ag_3^+ complex shows only minor frequency shifts with respect to the oxazole/water dimer in good agreement with the experimental observations on going from the aqueous solution to the physisorbed sample (see panel c of Figure 2). In addition, the calculated Raman intensities, shown in Figure 13, also satisfactorily reproduce the SERS spectrum of physisorbed oxazole with the exception of the band at ~1265 cm^{-1}, that is underestimated.

On the contrary, the larger frequency shifts observed in the chemisorbed oxazole (Figure 2d) are interpreted on the basis of a direct interaction of the molecule with silver and the formation of a chemical bond (Ag···N distance, 2.25 Å) between the lone pair of the nitrogen atom and positively charged adclusters of the metal surface.

This work shows the efficiency of a combined experimental and computational approach to understand both the physisorption and the chemisorption processes of organic molecules on metal colloidal nanoparticles and to correctly interpret the corresponding SERS spectra.

Acknowledgment. This work was supported by the Ministero dell'Istruzione, dell'Università e della Ricerca (MIUR).

References and Notes

(1) Somorjai, G. A. *Chem. Rev.* **1996**, *96*, 1223–1235.
(2) Jain, P. K.; Huang, X.; El-Sayed, I. H.; El-Sayed, M. A. *Acc. Chem. Res.* **2008**, *41*, 1578–1586.
(3) Odom, T. W.; Pileni, M. *Acc. Chem. Res.* **2008**, *41*, 1565.
(4) Otto, A. In *Light Scattering in Solids*; Cardona, M., Güntherodt, G., Eds.; Springer-Verlag: Berlin, 1984; Vol. IV.
(5) Aroca, R. *Surface-Enhanced Vibrational Spectroscopy*; J. Wiley and Sons: New York, 2006.
(6) Kneipp, K.; Moskovits, M.; Kneipp, H. *Surface-Enhanced Raman Scattering*; Springer-Verlag: Berlin, Germany, 2006.
(7) Jensen, L.; Aikens, C. M.; Schatz, G. C. *Chem. Soc. Rev.* **2008**, *37*, 1061–1073.
(8) Nie, S.; Emory, S. R. *Science* **1997**, *275*, 1102.
(9) Mrozek, I.; Otto, A. *J. Electron Spectrosc. Relat. Phenom.* **1990**, *54*, 895.
(10) Campion, A.; Ivanecky III, J. E.; Child, C. M.; Foster, M. *J. Am. Chem. Soc.* **1995**, *117*, 11807.
(11) Hohenberg, P.; Kohn, W. *Phys. Rev.* **1964**, *136*, B864.
(12) Kohn, W.; Sham, L. J. *Phys. Rev.* **1965**, *140*, A1133.
(13) Car, R.; Parrinello, M. *Phys. Rev. Lett.* **1985**, *55*, 2471–2474.
(14) Parrinello, M. *Solid State Commun.* **1997**, *102*, 107–120.
(15) Parrinello, M. *Comput. Sci. Eng.* **2000**, *2*, 22–27.
(16) Tse, J. S. *Annu. Rev. Phys. Chem.* **2002**, *53*, 249–290.
(17) Pagliai, M.; Bellucci, L.; Muniz-Miranda, M.; Cardini, G.; Schettino, V. *Phys. Chem. Chem. Phys.* **2006**, *8*, 171–178.
(18) Muniz-Miranda, M.; Cardini, G.; Pagliai, M.; Schettino, V. *Chem. Phys. Lett.* **2007**, *436*, 179–183.
(19) Muniz-Miranda, M.; Pagliai, M.; Cardini, G.; Schettino, V. *J. Phys. Chem. C* **2008**, *112*, 762–767.
(20) Otto, A. *J. Raman Spectrosc.* **2005**, *36*, 497–509.
(21) Xiong, Y.; Washio, I.; Chen, J.; Sadilek, M.; Xa, Y. *Angew. Chem., Int. Ed.* **2007**, *46*, 4917–4921.
(22) *Chemistry of Heterocyclic Compounds, Oxazole: Synthesis, Reactions and Spectroscopy*; Palmer, D. C., Ed.; Wiley-Interscience: Hoboken, NJ, 2003.
(23) Frisch, M. J. ; Trucks, G. W.; Schlegel, H. B.; Scuseria, G. E.; Robb, M. A.; Cheeseman, J. R.; Montgomery, J. A.; Jr.; Vreven, T.; Kudin, K. N.; Burant, J. C.; Millam, J. M.; Iyengar, S. S.; Tomasi, J.; Barone, V.; Mennucci, B.; Cossi, M.; Scalmani, G.; Rega, N.; Petersson, G. A.; Nakatsuji, H.; Hada, M.; Ehara, M.; Toyota, K.; Fukuda, R.; Hasegawa, J.; Ishida, M.; Nakajima, T.; Honda, Y.; Kitao, O.; Nakai, H.; Klene, M.; Li, X.; Knox, J. E.; Hratchian, H. P.; Cross, J. B.; Bakken, V.; Adamo, C.; Jaramillo, J.; Gomperts, R.; Stratmann, R. E.; Yazyev, O.; Austin, A. J.; Cammi, R.; Pomelli, C.; Ochterski, J. W.; Ayala, P. Y.; Morokuma, K.; Voth, G. A.; Salvador, P. J.; Dannenberg, J.; Zakrzewski, V. G.; Dapprich, S.; Daniels, A. D.; Strain, M. C.; Farkas, O.; Malick, D. K.; Rabuck, A. D.; Raghavachari, K.; Foresman, J. B.; Ortiz, J. V.; Cui, Q.; Baboul, A. G.; Clifford, S.; Cioslowski, J.; Stefanov, B. B.; Liu, G.; Liashenko, A.; Piskorz, P.; Komaromi, I.; Martin, R. L.; Fox, D. J.; Keith, T.; Al-Laham, M. A.; Peng, C. Y.; Nanayakkara, A.; Challacombe, M.; Gill, P. M. W.; Johnson, B.; Chen, W.; Wong, M. W.; Gonzalez, C.; Pople, J. A. *Gaussian 03, Revision C.02*, Gaussian, Inc., Wallingford CT, 2004.
(24) Hutter, J.; Alavi, A.; Deutch, T.; Bernasconi, M.; Goedecker, S.; Marx, D.; Tuckerman, M.; Parrinello, M. *CPMD*; MPI für Festkörperforschung and IBM Zurich Research Laboratory: Stuttgart, 1995−1999.
(25) Becke, A. D. *Phys. Rev. A* **1988**, *38*, 3098–3100.
(26) Lee, C.; Yang, W.; Parr, R. G. *Phys. Rev. B* **1988**, *37*, 785–789.
(27) Troullier, N.; Martins, J. L. *Phys. Rev. B* **1991**, *43*, 1993–2006.
(28) Kleinman, L.; Bylander, D. M. *Phys. Rev. Lett.* **1982**, *48*, 1425–1428.
(29) Becke, A. D. *J. Chem. Phys.* **1993**, *98*, 5648–5652.
(30) Stephens, P. J.; Devlin, F. J.; Chabalowski, C. F.; Frisch, M. J. *J. Phys. Chem.* **1994**, *98*, 11623–11627.
(31) Hertwig, R. H.; Koch, W. *Chem. Phys. Lett.* **1997**, *268*, 345–351.
(32) Hay, P. J.; Wadt, W. R. *J. Chem. Phys.* **1985**, *82*, 270–283.

(33) Hay, P. J.; Wadt, W. R. *J. Chem. Phys.* **1985**, *82*, 299–310.
(34) Wadt, W. R.; Hay, P. J. *J. Chem. Phys.* **1985**, *82*, 284–298.
(35) Jensen, F. *Introduction to Computational Chemistry*; J. Wiley and Sons, LTD: New York, 2007.
(36) Foresman, J. B.; Frisch, A. *Exploring Chemistry with Electronic Structure Methods*; Gaussian, Inc.: Pittsburgh, PA, 1996.
(37) Wilson, Jr.; E. B.; Decius, J. C.; Cross, P. *Molecular Vibrations*; Dover Publications, Inc.: New York, 1980.
(38) Creighton, J. A.; Blatchford, C. G.; Albrecht, M. G. *J. Chem. Soc., Faraday Trans. II* **1979**, *75*, 790–798.
(39) Muniz-Miranda, M. *Vib. Spectrosc.* **1999**, *19*, 227–232.
(40) McDonald, N. A.; Jorgensen, W. L. *J. Phys. Chem. B* **1998**, *102*, 8049–8059.
(41) Laasonen, K.; Sprik, M.; Parrinello, M.; Car, R. *J. Chem. Phys.* **1993**, *99*, 9080–9089.
(42) Silvestrelli, P. L.; M., P. *J. Chem. Phys.* **1999**, *111*, 3572–3580.
(43) Izvekov, S.; Voth, G. A. *J. Chem. Phys.* **2002**, *116*, 10372–10376.
(44) Kuo, I.-F. W.; Mundy, C. J.; McGrath, M. J.; Siepmann, J. I.; VandeVondele, J.; Sprik, M.; Hutter, J.; Chen, B.; Klein, M. L.; Mohamed, F.; Krack, M.; Parrinello, M. *J. Phys. Chem. B* **2004**, *108*, 12990–12998.
(45) Pagliai, M.; Cardini, G.; Righini, R.; Schettino, V. *J. Chem. Phys.* **2003**, *119*, 6655–6662.
(46) Handgraaf, J.; van Erp, T. S.; Meijer, E. J. *Chem. Phys. Lett.* **2003**, *367*, 617–624.
(47) Schettino, V.; Chelli, R.; Marsili, S.; Barducci, A.; Faralli, C.; Pagliai, M.; Procacci, P.; Cardini, G. *Theor. Chem. Acc.* **2007**, *117*, 1105–1120.
(48) Desiraju, G. R.; Steiner, T. *The Weak Hydrogen Bond*; Oxford University Press: New York, 1999.
(49) Luzar, A.; Chandler, D. *Phys. Rev. Lett.* **1996**, *76*, 928–931.
(50) Svishchev, I. M.; Kusalik, P. G. *J. Chem. Phys.* **1993**, *99*, 3049–3058.
(51) Pagliai, M.; Cardini, G.; Schettino, V. *J. Phys. Chem. B* **2005**, *109*, 7475–7481.
(52) Faralli, C.; Pagliai, M.; Cardini, G.; Schettino, V. *J. Phys. Chem. B* **2006**, *110*, 14923–14928.
(53) Sing, D.; Srivastava, S. K.; Ojha, A. K.; Asthana, B. P.; Singh, R. K. *J. Mol. Struct. (Theochem)* **2007**, *819*, 88–94.
(54) Ohmine, I.; Saito, S. *Acc. Chem. Res.* **2006**, *32*, 741.
(55) Tsai, K. H.; Wu, T.-M. *Chem. Phys. Lett.* **2006**, *417*, 389–394.
(56) Walrafen, G. E. *J. Phys. Chem.* **1999**, *94*, 2237–2239.
(57) Kraka, E.; Cremer, D.; Sproerel, U.; Merke, I.; Stahl, W.; Dreizler, H. *J. Phys. Chem.* **1995**, *99*, 12466–12477.
(58) Palmer, M. H. *J. Mol. Struct.* **2007**, *834*−*836*, 113–128.
(59) van Duijneveldt, F. B.; van Duijneveldt-van de Rijdt, J. G. C. M.; van Lenthe, J. H. *Chem. Rev.* **1994**, *94*, 1873–1885.

JP905530X